Applied Mechanics and Materials Vol. 419 (2013) pp 23-29

doi:10.4028/www.scientific.net/AMM.419.23

Normal force computation for axisymmetric multistage launch vehicle

Laith K. ABBAS [1,a], Dong-yang CHEN[1,b] and Xiao-ting RUI[1,c]

[1]Institute of Launch Dynamics, Nanjing University of Science and Technology, Nanjing, 210094, China

[a]laithabbass@yahoo.com, [b]cdy_1988@sina.cn, [c]ruixt@163.net

Keywords: Computational fluid dynamics, Normal force coefficient, Structured grid, Multistage launch vehicle.

Abstract. The increased demand upon the aeroelastician to obtain the distributed aerodynamic normal force loads for arbitrary launch vehicle configurations necessitated accurate method. In this work, computational fluid dynamics (CFD) is used for the determining the distributed aerodynamic loads of an axisymmetric multistage launch vehicle in the linear angle-of-attack range. ICEM-CFD and ANSYS-FLUENT software are implemented for the meshing and computational analysis. About 2750 iterations were used for the simulation purpose. Computational results are compared to available experimental data. In general, a good result within engineering error margins is obtained.

Introduction

Launch vehicles are typically designed to fly at low angles of attack. Nevertheless, even at such low angles, the lateral loads that arise in these vehicles are quite strong, and they must be accurately determined [1]. Moreover, the effects of body flexibility have been increasingly recognized as important factors in the dynamic loads and stability studies performed on the aerospace configurations. The inclusion of body flexibility has introduced the need for an adequate description of the distributed aerodynamic loads acting on the deformed body. The efforts required to obtain distributed data are considerably greater than those for obtaining total aerodynamic coefficients. However, the distributed aerodynamic data are essential to the adequate analysis of aeroelastic divergence, aeroelastic feedback coupling of closed-loop autopilot systems, flight dynamic stability characteristics necessary for the control system design, and dynamic loads of flexible structures experiencing atmospheric disturbances. The severity of such instabilities and the load magnifications due to flexibility justify the extensive efforts required in generating appropriate distributed aerodynamics. Unfortunately, the ability to determine distributed aerodynamic loadings has not increased at the same rate as the need for such data [2].

Over the last few decades, computational fluid dynamics (CFD) has developed into a rich and diverse subject and is emerged as a major component of applied and basic fluid dynamic research along with theoretical and experimental studies. Simultaneous development of new computers, numerical algorithms, physical and chemical models of flow physics are responsible for the great impact of CFD in both basic and applied scientific / engineering problems. Presently, CFD methods are employed routinely for the estimation of various complex aerodynamic and propulsion flow parameters where experimental data cannot be obtained economically or feasibly. CFD has emerged as one of the important design tools along with the wind tunnels and other experimental testing and contributing significantly in reducing developmental cost and time for aerospace vehicle design.

In this paper, ANSYS-FLUENT, which represents a powerful tool of CFD for thermo fluids analysis and has been designed to use in a CAE environment is used for determining the distributed aerodynamic loads of an axisymmetric multistage launch vehicle in the linear operational range of angle-of-attack. A computational result is compared to available experimental data. In general, a good result within engineering error margins is obtained.

CFD governing equations

For any CFD problem, the general transport equation for property ϕ (general variable) is [3]

$$\underbrace{\partial(\rho\phi)/\partial t}_{\substack{\text{Rate of increase of}\\ \phi \text{ of fluid element}}} + \underbrace{\operatorname{div}(\rho\phi\mathbf{u})}_{\substack{\text{Net rate of flow of}\\ \phi \text{ out of fluid element}}} = \underbrace{\operatorname{div}(\Gamma \operatorname{grad}\phi)}_{\substack{\text{Rate of increase of}\\ \phi \text{ due to diffusion}}} + \underbrace{S_\phi}_{\substack{\text{Rate of increase of}\\ \phi \text{ due to sources}}} . \tag{1}$$

Where ρ is the density, t is the time and $\mathbf{u}$ is the velocity vector. It clearly highlights the various transport processes: the *rate of change* term and the *convective* term on the left-hand side and the *diffusive* term (Γ=diffusion coefficient) and the *source* term respectively on the right-hand side. In order to bring out the common features we have, of course, had to hide the terms that are not shared between the equations in the source terms. Note that Eq. (1) can be made to work for the governing equations according to the symbols of each particular equation, i.e. Continuity equation, momentum equations and energy equation by setting $\phi = 1, \Gamma = S_\phi = 0; \phi = u_i, \Gamma = \mu, S_\phi = -\partial p/\partial x_i + S_M$; $\phi = T, \Gamma = k/C_v$ $S_\phi = -p \operatorname{div}\mathbf{u} + \Phi + S_i$, respectively. Herein, Φ is the dissipation function, $u_i \equiv (u_1 = u, u_2 = v, u_3 = w)$ is the velocity components in the direction $x_i \equiv (x_1 = x, x_2 = y, x_3 = z)$, C_v is the specific heat, k is the Boltzmann constant relating temperature T and energy, p is the pressure and S_M is the momentum source. Equation (1) is used as the starting point for computational procedures in the finite volume method by integrating the differential equation, and then to apply "Gauss divergence theorem", which for a vector a states $\int_{CV} \operatorname{div}(\mathbf{a}) = \int_A \mathbf{n}\cdot\mathbf{a}\,\mathrm{d}A$ .This then leads to the following general conservation equation in integral form

$$\underbrace{\partial/\partial t \int_{CV} \rho\phi \,\mathrm{d}V}_{\text{Rate of increase of } \phi} + \underbrace{\int_A \mathbf{n}\cdot(\rho\phi\mathbf{u})\,\mathrm{d}A}_{\substack{\text{Net rate of decrease of } \phi \text{ due to}\\ \text{convection across boundaries}}} = \underbrace{\int_A \mathbf{n}\cdot(\Gamma \operatorname{grad}\phi)\,\mathrm{d}A}_{\substack{\text{Net rate of increase of } \phi \text{ due to}\\ \text{diffusion across boundaries}}} + \underbrace{\int_{CV} S_\phi \,\mathrm{d}V}_{\text{Net rate of creation of } \phi} . \tag{2}$$

This is the actual form of the conservation equations solved by finite volume based CFD programs to calculate the flow pattern and associated scalar fields.

Most researchers are intuitively aware that the fluid flow of both gases and liquids is inherently transient (unsteady) by nature. As an example, just ponder the movement of leaves on a tree in a breeze or the flow of water from a tap. Less intuitive is that even a relatively steady flow in a wind tunnel has transient velocities that vary at scales and frequencies that our human senses are unable to discern. Such variations are known as turbulence. The treatment of turbulence in the Reynolds-Averaged Navier-Stokes (RANS) equations lies at the heart of most practical CFD approaches. Decomposing the Navier-Stokes (NS) equations into the RANS equations makes it possible to simulate practical engineering flows, such as the airflow over aerospace vehicles. The assumption (known as the Reynolds decomposition) behind the RANS equations is that the time-dependent turbulent (chaotic) velocity fluctuations can be separated from the mean flow velocity. The Reynolds decomposition defines flow property f at this point as the sum of a steady mean component $\overline{f}$ and a time varying fluctuating component $f'(t)$ with zero mean value, i.e. $f = \overline{f} + f'(t)$. All other flow variables, i.e. all other velocity components, the pressure, temperature, density etc., will also exhibit this additional time-dependent behavior ($\mathbf{u} = \mathbf{U} + \mathbf{u}' \equiv u = U + u'; v = V + v'; w = W + w'$ and $p = P + p'$). Using averaging and substitution in Eq. 1, RANS equations end up with the following forms

$$\frac{\partial\rho}{\partial t} + \frac{\partial(\rho\overline{u}_i)}{\partial x_i} = 0,$$
$$\frac{\partial(\rho\overline{u}_i)}{\partial t} + \frac{\partial(\rho\overline{u}_i\overline{u}_j)}{\partial x_j} = -\frac{\partial\overline{p}}{\partial x_i} + \frac{\partial}{\partial x_j}\left[2\mu\left(S_{ij} - \frac{1}{3}S_{kk}\delta_{ij}\right)\right] + \frac{\partial}{\partial x_j}(-\rho\overline{u_i'u_j'}) \quad \text{where } -\rho\overline{u_i'u_j'} = R_{ij};\ \ S_{ij} = \frac{1}{2}\left(\frac{\partial\overline{u}_i}{\partial x_j} + \frac{\partial\overline{u}_j}{\partial x_i}\right). \tag{3}$$

The viscosity, μ, is the property of the fluid and S_{ij} is the instantaneous strain rate tensor. Eq.3 then introduces a set of unknowns called the Reynolds stresses (R_{ij}) which are functions of the velocity fluctuations. The reduced computational requirements for the RANS equations, while still significant, are orders of magnitude less than that required for the original NS equations. Another advantage of using the RANS equations for steady fluid flow simulation is that the mean flow velocity is calculated as a direct result without the need to average the instantaneous velocity over a series of time steps. Therefore, the objective of the turbulence models for RANS equations is to compute R_{ij} to closure Eq.3. This can be done by one of three main categories of RANS-based turbulence models, namely, linear eddy viscosity, nonlinear eddy viscosity and Reynolds stress. In present research, shear stress transport (SST) $k-\omega$ turbulence model (integrates the advantages of $k-\varepsilon$ and $k-\omega$ models) developed by Menter [4, 5] is considered for R_{ij} computations. Boussinesq hypothesis is utilized in Eq. (3) to relate R_{ij} to the mean velocity gradients within the flow, i.e., $-\rho\overline{u_i'u_j'}=\mu_t\left(\frac{\partial\overline{u}_i}{\partial x_j}+\frac{\partial\overline{u}_j}{\partial x_i}\right)-\frac{2}{3}\left(\rho k+\mu_t\frac{\partial\overline{u}_k}{\partial x_k}\right)\delta_{ij}$, where, $\mu_t=\rho k/\omega$ is the turbulent (or eddy) viscosity and k is the turbulent kinetic energy. For two-equation turbulence models such as the $k-\varepsilon$ and $k-\omega$ variants, the turbulent viscosity is computed through the solution of two additional transport equations for the turbulent kinetic energy and the specific dissipation rate, $\omega=\varepsilon/k$, where ε is the turbulence dissipation rate. Moreover, the SST $k-\omega$ is more accurate and reliable for a wider class of flows than the standard $k-\omega$, including adverse pressure gradient and separation flow. Menter's SST model is based on a mix of two equations $k-\varepsilon$ and $k-\omega$ turbulence models using a blending function F_1. The model can be written as [4]

$$\underbrace{\frac{\partial}{\partial x_i}(\rho k u_i)=\frac{\partial}{\partial x_j}\left[\left(\mu+\frac{\mu_t}{\sigma_k}\right)\frac{\partial k}{\partial x_j}\right]+G_k-Y_k}_{\text{Turbulence kinetic energy } k\text{ -equation}};\quad \underbrace{\frac{\partial}{\partial x_i}(\rho\omega u_i)=\frac{\partial}{\partial x_j}\left[\left(\mu+\frac{\mu_t}{\sigma_\omega}\right)\frac{\partial\omega}{\partial x_j}\right]+G_\omega-Y_\omega}_{\text{Specific dissipation rate } \omega\text{-equation}};$$

$$\sigma_k=\frac{1}{F_1/\sigma_{k,1}+(1-F_1)/\sigma_{k,2}};\ \sigma_\omega=\frac{1}{F_1/\sigma_{\omega,1}+(1-F_1)/\sigma_{\omega,2}};\ F_1=\tanh\left(\Phi_1^4\right);\ G_k=\mu_t S^2;\ S\equiv\sqrt{2S_{ij}S_{ij}};$$

$$\Phi_1=\min\left[\max\left(\frac{\sqrt{k}}{0.09\omega y},\frac{500\mu}{\rho y^2\omega}\right),\frac{4\rho k}{D_\omega^+\sigma_{\omega,2}y^2}\right];\ D_\omega^+=\max\left[2\rho\frac{1}{\sigma_{\omega,2}}\frac{1}{\omega}\frac{\partial k}{\partial x_j}\frac{\partial\omega}{\partial x_j},10^{-20}\right];\ G_\omega=\frac{\gamma_\infty}{\nu_t}G_k;$$

$$\gamma_\infty=F_1\gamma_{\infty,1}+(1-F_1)\gamma_{\infty,2};\ \gamma_{\infty,1}=\frac{\beta_{i,1}}{\beta_\infty^*}-\frac{k^2}{\sigma_{\omega,1}\sqrt{\beta_\infty^*}};\ \gamma_{\infty,2}=\frac{\beta_{i,2}}{\beta_\infty^*}-\frac{k^2}{\sigma_{\omega,2}\sqrt{\beta_\infty^*}};\ \nu_t=\frac{0.31k}{\max(0.31\omega,\Omega F_2)};$$

$$F_2=\tanh\left(\Phi_2^2\right);\ \Phi_2=\max\left(2\frac{\sqrt{k}}{0.09\omega y},\frac{500\mu}{\rho y^2\omega}\right);\ Y_k=\rho\beta^*k\omega;\ Y_\omega=\rho\beta_i\omega^2;\ \beta_i=F_1\beta_{i,1}+(1-F_1)\beta_{i,2};$$

$$\sigma_{k,1}=1.176;\ \sigma_{\omega,1}=2.0;\ \sigma_{k,2}=1.0;\ \sigma_{\omega,2}=1.168;\ \beta_{i,1}=0.075;\ \beta_{i,2}=0.0828;\ \beta^*=0.09. \tag{4}$$

CFD codes are structured around the numerical algorithms that can tackle fluid flow problems. In general, the pre-processor contains applications and tools to provide the required boundary conditions for the analysis and the calculations were performed by the solver. The results of the flow field and other aerodynamic force were obtained using the post-processor [6]. Solving the RANS equations with SST turbulent model, density, velocity, pressure, etc could be computed at every grid node. Then, normal, axial, lift, and drag coefficients can be obtained, respectively

$$C_N=N/q_\infty S_{ref};\ C_A=A/q_\infty S_{ref};\ C_L=C_N\times\cos\alpha-C_A\times\sin\alpha;\ C_D=C_N\times\sin\alpha+C_A\times\cos\alpha. \tag{5}$$

where q_∞, α and S_{ref} are the dynamic pressure, angle of attack and reference area, respectively.

Simulation and discussion

Creating the model: Pre-processing stage

Space vehicle as a body may be comprised of various geometrical components such as spheres, cones, cylinders, cone frustums, and other bodies of revolution generated by given arcs. An axisymmetric multistage launch vehicle [7] under investigation in the present work is shown in Fig. 1 and operating in supersonic speeds and angle-of-attack up to 5°. The body consists of four parts, namely; cone with semi-vertex angle $\theta_N = 15^{\circ}$, mid cylinder with diameter $D_1 = 1.67\text{m}$, cone frustum with angle $\theta_F = 5^{\circ}$ and aft cylinder with diameter $D_2 = 2.4\text{m}$. Longitudinally, the body is divided into 22 segments as tabulated in Table 1. The middle point of each section is the normal force action point. For its simplicity and faster, SpaceClaim 3D software is used to establish the geometry of the body (see Fig. 2) according to Table 1 and imported to ICEM CFD using the PARASOLID format.

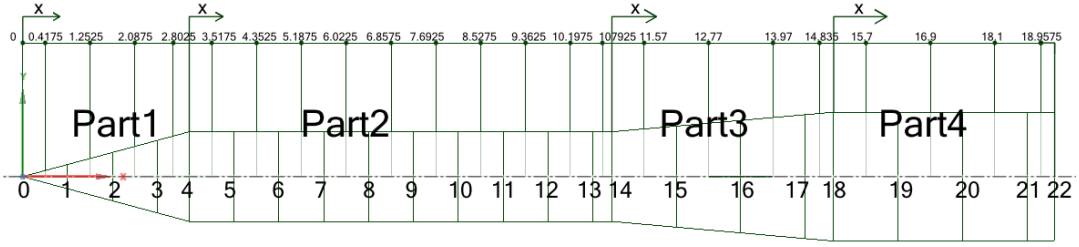

Fig. 1 Longitudinal division of the multistage vehicle (in meters).

Table 1 Vehicle segmentation.

Part 1	**0**	**1**	**2**	**3**	**4**					
x/D_1	**0**	**0.5**	**1**	**1.5**	**1.8563**					
Part 2	**5**	**6**	**7**	**8**	**9**	**10**	**11**	**12**	**13**	**14**
x/D_1	**0.5**	**1**	**1.5**	**2**	**2.5**	**3**	**3.5**	**4**	**4.5**	**4.7126**
Part 3	**15**	**16**	**17**	**18**						
x/D_2	**0.5**	**1**	**1.5**	**1.721**						
Part 4	**19**	**20**	**21**	**22**						
x/D_2	**0.5**	**1**	**1.5**	**1.7146**						

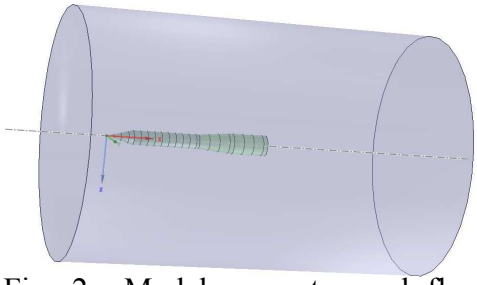

Fig. 2 Model geometry and flow control volume.

The body has the far-field boundary located at about $2D_2$ upstream away from the body-nose, about $8D_2$ away from the body-bottom downstream, and about $6D_2$ away from the body-surface in a lateral. It is important to place the far-field boundary far enough from the object of interest since we are using the ambient conditions to define the boundary conditions at the far-field.

Flow grid: Pre-processing stage

The meshing of the flow is performed using ICEM CFD software through the following steps. Firstly, generate multi-block for the control volume as shown in Fig. 3(a). This is a good privilege to improve the mesh quality and take the exact shape of the body. Use the O-block topology to generate the structured boundary layer blocks around the body block as shown in Fig. 3(b). Then, meshing the flow and check quality of the mesh. The maximum aspect ratio is quite high in this mesh. This is because the gird cells are very close to the body wall surfaces. It's required for the turbulence model being used to ensure the first grid point is in the viscous sublayer (y^+).White [8] divided the turbulent boundary layer into four different layers as follows: viscous sublayer ($y^+ \le 5$), buffer layer ($5 \le y^+ \le 30$), overlap layer ($30 \le y^+ \le 350$) and outer layer ($y^+ \ge 350$). The limits of different layers vary in the literature. Also the limits of these regions vary with the Reynolds number, especially the

upper limit of the overlap layer. Thus, these values should be regarded as guidelines, not definitions. In this work, $y^+ = 5$ which gives 708 blocks, 1209828 nodes, 1193790 hexahedral cells and 3565500 quadrilateral interior faces. The final generated flow gird mesh is shown in Fig. 3(c).

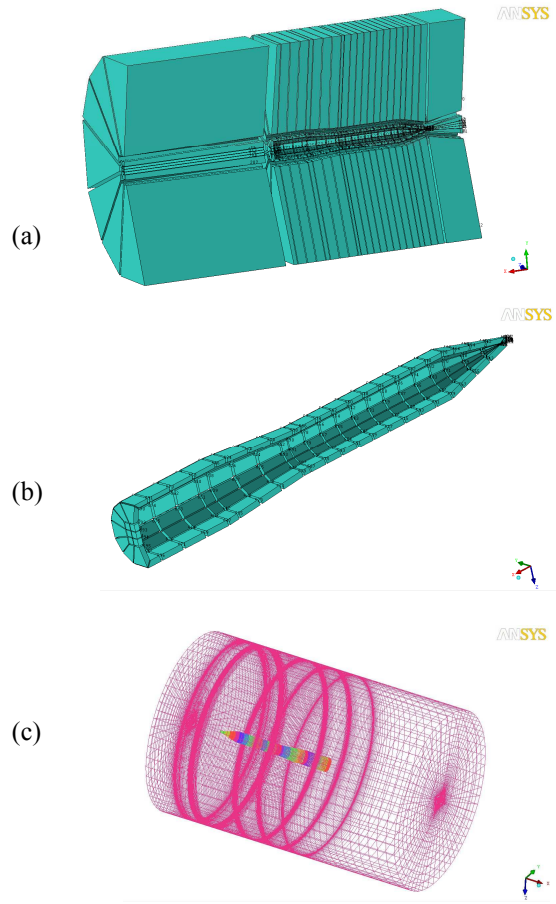

Fig.3 Meshed the control volume. (a)multi-block (b)O-block topology (c) flow field computation grid.

Boundary conditions, solution schemes and simulation: Processing stage

The meshed body was imported into ANSYS-FLUENT and simulated. The mesh was checked for errors. The solver used is steady-state density based solver. Energy equation is used for the simulation because the flow is compressible and also idea gas equation is used. The two-equation SST $k-\omega$ turbulent model is chosen. In this work, the outer boundaries were set as far-field, with sea level condition. The air is assumed as an ideal gas and the viscosity varies with temperature in accordance with Surthland three coefficient formulas. The far-field boundary is based on Riemann invariants reflecting boundary conditions. For compressible flow, $P_{total} = P_{static}(1+\frac{\gamma-1}{2}M^2)^{\frac{\gamma}{\gamma-1}}$ and $T_{total} = T_{static}(1+\frac{\gamma-1}{2}M^2)^{\frac{\gamma}{\gamma-1}}$, where M is flight Mach number, and γ is the adiabatic exponent. The solution method is implicit formulation and Advection Upstream Splitting Method (AUSM). The implicit formulation for time discretization is more stable and can be driven much harder to reach a converged solution in less time. AUSM which is based on the finite volume method and is used to Spatial discrete the space of fluid field. The least square cell based gradient method is used. Second Order Upwind scheme is used on convection and turbulent viscosity terms. The Courant number (CFL) determines the internal time step and affects the solution speed and stability. The CFL for the density-based implicit formulation is 5. It is often possible to increase the CFL, depending on the complexity of problem, but it can be changed as the solution progresses. The input data then is setup for ambient condition (sea level) such as pressure and temperature (101.325kPa, 288 K). Setting $\gamma = 1.4, M = 2.36$ and $\alpha = 3^0$, the simulation is proceeded with a maximum number of iterations 5000. The computations took about 4 seconds/iteration, using 32GB (RAM) and INTEL Xeon E5649 processor. Total computation was performed less than 4 hours. Convergence was determined by tracking the change in the solver graph displayed in the FLUENT environment. Then the simulation will stop. The solution was deemed converged when the lift and drag coefficients had stabilized around 2750 iterations as shown in Fig. 4 (a, b).

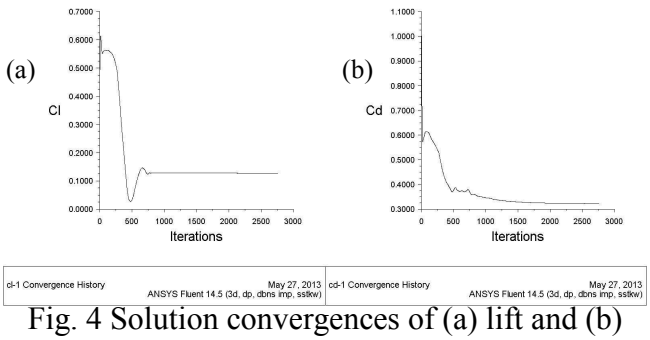

Fig. 4 Solution convergences of (a) lift and (b) drag coefficients.

Output: Post-processing stage

In the post processing, the CFD results of pressure and velocity counters are shown in Fig. 5(a, b), respectively. Fig. 5 (c) illustrates the distributed normal force coefficient slope ($S_{ref}\frac{dC_{N\alpha}}{dx}$) which obtained in the range of linear angle-of-attack. Within the engineering error margins, the whole distribution along the vehicle's length demonstrates a good result in comparison with the experimental wind tunnel data (Fig. 5(d) [7]).

Summery

Computational results using ANSYS-FLUENT were presented to show the distribution of the aerodynamic normal force coefficient for axi-symmetric multistage vehicle can be predicted well in comparison to the wind-tunnel data. The distributed aerodynamic data are essential to the adequate analysis of aeroelasticity, flight dynamic stability characteristics and dynamic loads of flexible structures experiencing atmospheric disturbances.

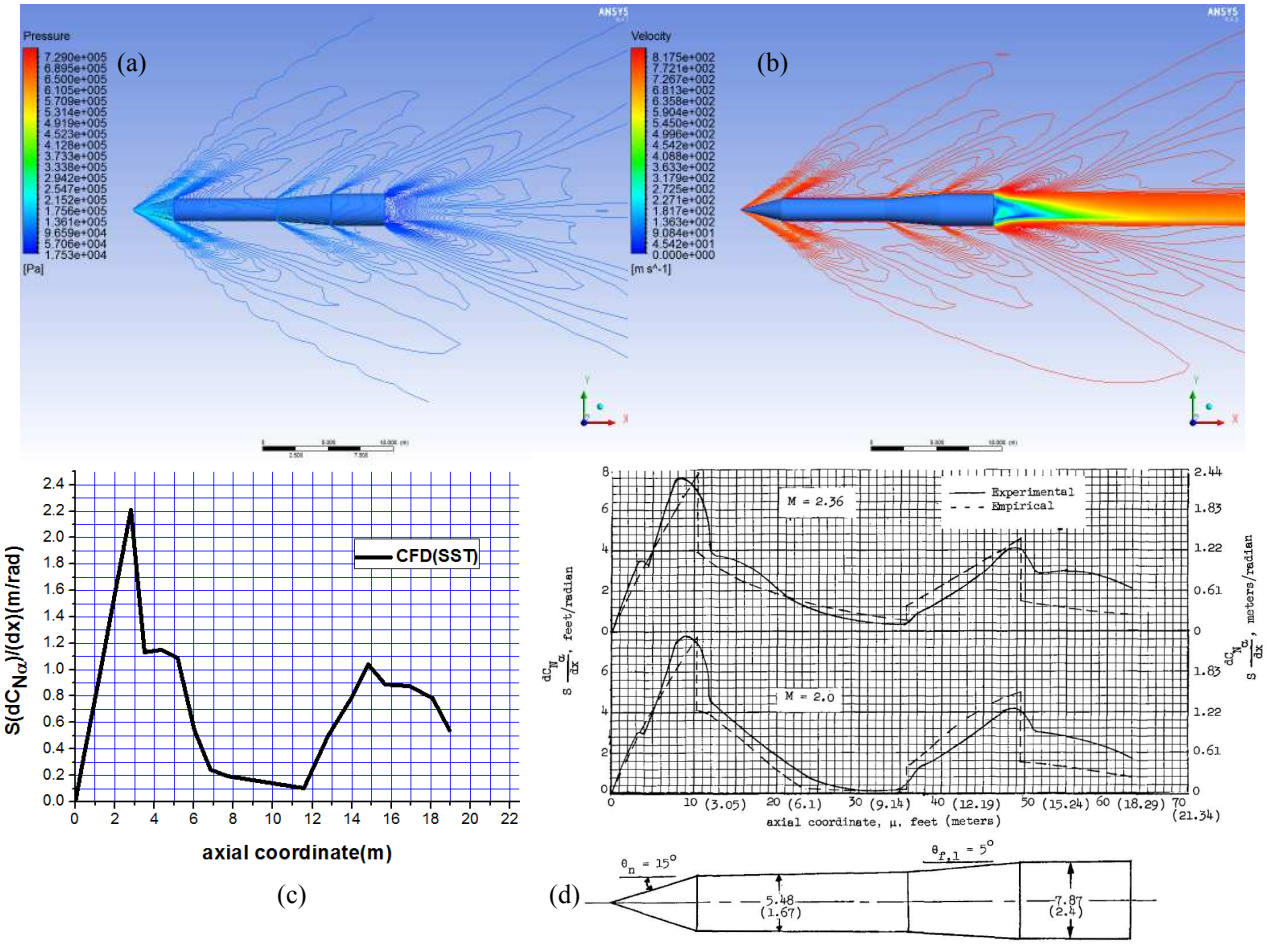

Fig. 5 (a) CFD: pressure counter (b) CFD: velocity counter (c) CFD: distributed normal force coefficient slope along vehicle length at $M = 2.36, \alpha = 3^{\circ}$ (d) experimental and empirical data for typical multistage launch vehicle [7].

References

[1] E. D. V. Bigarella, J. L. F. Azevedo, O. A. F. Mello, Normal force calculations for rocket-like configurations. Journal of the Brazilian Society of Mechanical Science and Engineering, 26(2004) 290-296.

[2] R. J. Muraca, An empirical method for determining static distributed aerodynamic loads on axisymmetric multistage launch vehicles. NACA TN D-3283 (1966).

[3] H. K. Versteeg, W. Malalasekera. An Introduction to Computational Fluid Dynamics: The Finite Volume Method, 2nd edition. Pearson Education Limited, United Kingdom, 2007.

[4] F. R. Menter, Zonal two equation k-ω turbulence models for aerodynamic flows. AIAA-93-2906 (1993).

[5] F. R. Menter, Two-equation eddy-viscosity models for engineering applications. AIAA Journal, 32(1994) 1598-1605.

[6] K. M. Bak, Experimental investigation and computational fluid dynamics analysis of missile with grid fin in subsonic flow. International Journal of Engineering Science and Technology, 2(2010) 6214-6220.

[7] R. B. Madden, Computing program for axial distribution of aerodynamic normal force characteristics for axisymmetric multistage launch vehicles. NASA TN D-4342 (1968).

[8] F. M. White, Viscous Fluid Flow, 2nd edition. McGraw-Hill Book Co., New York,1991.